Applied Physics Letters

Solution-based SnGaO thin-film transistors for Zn- and In-free oxide electronic devices

Cite as: Appl. Phys. Lett. **113**, 122101 (2018); https://doi.org/10.1063/1.5046119
Submitted: 26 June 2018 . Accepted: 03 September 2018 . Published Online: 18 September 2018

Zhaogui Wang, Jiwen Zheng, Minmin Li, Qian Wu, Bolong Huang, Changdong Chen, Jin Wu, and Chuan Liu

ARTICLES YOU MAY BE INTERESTED IN

High mobility ultra-thin crystalline indium oxide thin film transistor using atomic layer deposition
Applied Physics Letters **113**, 112102 (2018); https://doi.org/10.1063/1.5041029

Yttrium zinc tin oxide high voltage thin film transistors
Applied Physics Letters **113**, 132101 (2018); https://doi.org/10.1063/1.5048992

Metal oxide semiconductor thin-film transistors for flexible electronics
Applied Physics Reviews **3**, 021303 (2016); https://doi.org/10.1063/1.4953034

Lock-in Amplifiers up to 600 MHz

© 2018 Author(s).

AIP Publishing

Solution-based SnGaO thin-film transistors for Zn- and In-free oxide electronic devices

Zhaogui Wang,[1] Jiwen Zheng,[1] Minmin Li,[1] Qian Wu,[1] Bolong Huang,[2] Changdong Chen,[1] Jin Wu,[1] and Chuan Liu[1,a)]

[1]*State Key Laboratory of Optoelectronic Materials and Technologies and The Guangdong Province Key Laboratory of Display Material and Technology, School of Electronics and Information Technology, Sun Yat-sen University, Guangzhou 510275, China*

[2]*Department of Applied Biology and Chemical Technology, The Hong Kong Polytechnic University, Hung Hom, Kowloon, Hong Kong and The Hong Kong Polytechnic University Shenzhen Research Institute, Shenzhen 518057, China*

(Received 26 June 2018; accepted 3 September 2018; published online 18 September 2018)

Oxide-based electronics call for low-cost and stable semiconductors to reduce cost and enable long-term operations. Transistors based on Sn show high field-effect mobility but generally exhibit weak stability and difficulty in solution-processed patterning. Here, we report solution-processed tin-gallium-oxide (SnGaO) thin-film transistors (TFTs) for In- and Zn-free electronics. Different from tin oxide, the amorphous SnGaO semiconductor features a wide bandgap of 4.6 eV, can be wet-etched and patterned by photolithography, and exhibits a large on-off ratio and good device stability in TFTs. The films are deposited via a sol-gel process and, in the photoelectron spectra, they exhibit typical signals of Sn^{4+} and Ga^{3+}, which act as the electron provider and suppresser, respectively. By varying the elemental ratios, the average field-effect mobility could be well controlled over a wide range from 0.66 to 9.82 cm^2/V s, the maximum mobility can reach 12 cm^2/V s, and the on/off ratio is above 10^6. The devices exhibited good stability for positive and negative bias stressing as well as with illumination, probably attributed to Ga-O bonds which are stronger than the weak Zn-O bonds. The presented studies may provide useful information to understand thin-film devices based on tin oxide and gallium oxide semiconductors. *Published by AIP Publishing.* https://doi.org/10.1063/1.5046119

Amorphous metal-oxide semiconductors (AMOSs) have drawn increasing attention in recent years due to their high carrier mobility, high transparency to visible light, large-scale uniformity, good stability, and low processing temperatures.[1,2] Based on AMOSs, various thin-film transistors (TFTs) have been demonstrated and studied, such as indium gallium zinc oxide (IGZO),[3,4] indium zinc oxide (IZO),[5,6] indium oxide (In_2O_3),[7] and indium zinc tungsten oxide (IZWO).[8] To reduce the cost of materials, In-free TFTs are worth studying for both fundamental science and application considerations, and Sn-based AMOSs have been considered a promising alternative since Sn and In have similar electronic configurations $[\mathrm{Kr}](4d)^{10}(5s)^{0}$.[9]

Various TFTs have been demonstrated based on Sn-based AMOSs including ZnSnO,[10,11] ZrZnSnO,[12,13] BaZnSnO,[14] and MgZnSnO.[15] Most of these materials include Zn, which has been found to probably cause instability in TFTs due to the weak Zn-O bonds.[16] To replace Zn and improve device stability, we consider using Ga as a carrier suppressor with Sn because the oxygen affinity of Ga is higher than those of Zn and Sn, and Ga_2O_3 shows a larger formation energy for oxygen vacancies than ZnO and SnO_2.[17,18] In addition, most of the Sn-based and Zn-free oxide TFTs were manufactured by vacuum processes,[19–21] which means high cost and complicated processes. In this paper, we study a SnGaO-based TFT fabricated by solution processing, and the fabrication is fully compatible with conventional photolithography.

The SnGaO precursor solutions were prepared by mixing gallium nitrate hydrate and tin chloride dihydrate in 2-methoxyethanol solvent with acetylacetone as a solution stabilizer. The total concentration of the metal precursors was fixed at 0.12 M, with molar ratios of Ga to the total contents (Ga and Sn) of 41.7%, 45.4%, 45.8%, 50.0%, and 54.2%, respectively. The spin-coated films were then pre-baked at 180 °C for 10 min to remove residual solvent, followed by annealing for 2 h at 350 °C to decompose and oxidize the precursors.[22] The films were patterned by photolithography using hydrochloric acid solution to etch and annealed at 350 °C afterwards. The chemical bonding in the SnGaO film was analyzed using XPS spectra (Fig. 1). The typical signals for Sn3d, O1s, and Ga2p were found at 486.9 eV, 530.7 eV, and 1118.1 eV, respectively. These signals correspond to mainly Sn^{4+} and Ga^{3+}, which are supposed to act as the provider and suppressor of free electrons, respectively.[9] Correspondingly, the film is mainly composed of SnO_2 and Ga_2O_3, and the ideal ionic bonding is presented schematically in Fig. 1(a).

The transmittance of SnGaO films on a quartz substrate was measured [Fig. 1(c)]; the data show a transmittance of over 90% from 310 nm to 800 nm, covering the spectral range from the near ultraviolet to visible light. The optical bandgap was determined using the absorption spectra of the films. The optical absorbance (α) and the optical bandgap (E_g) are related by the following equation:[23] $(\alpha h\nu)^2 = C(h\nu - E_g)$. Here, the parameters h, ν, and C are the Planck constant, frequency of the incident photon, and a constant, respectively. Accordingly, an optical bandgap for the SnGaO films is

a)E-mail: liuchuan5@mail.sysu.edu.cn

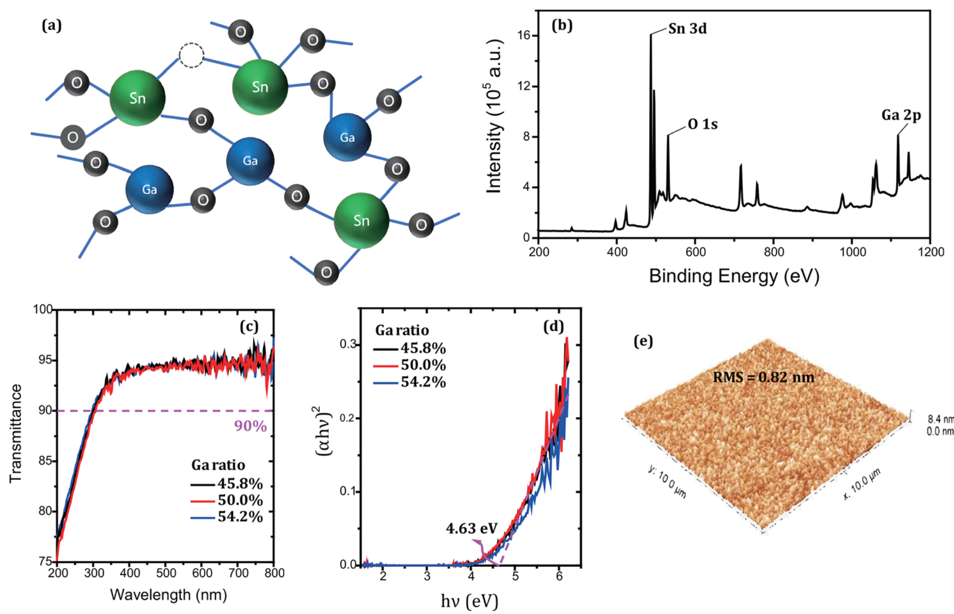

FIG. 1. (a) Schematic representations of the ionic bonding in an ideal SnGaO system. (b) XPS survey spectrum showing characteristic peaks for Sn, Ga, and O. (c) Optical transmittance spectra for SnGaO films with different Ga ratios. (d) Plots of $(\alpha h\nu)^2$ vs $h\nu$. (e) AFM scanning image of the film surface.

4.63 eV for 50.0% Ga [Fig. 1(d)], between the bandgap of SnO_2 (3.6 eV)[24] and Ga_2O_3 (4.8 eV).[25] Furthermore, X-ray diffraction patterns were examined and no crystallization peaks were observed, which confirms that the SnGaO films are amorphous. The film was scanned using an Atomic Force Microscope (AFM) and generally exhibited a continuous, smooth surface with a measured root mean square (RMS) roughness of 0.82 nm [Fig. 1(e)], which is small when comparing to the film thickness as 15–20 nm. Such a thickness is similar to those of other previously reported oxide transistors.[26]

For TFT fabrication, *n*-doped Si, 100 nm thick SiO_2, and 40 nm thick Al were gate, dielectric, and source/drain electrodes, respectively. The channel width and length of the devices characterized were 1000 and 250 μm, respectively. There are 35 devices on a 2×2 cm substrate. The bottom-gate, top-contact TFTs with various compositional ratios (Fig. 2) exhibit different transfer characteristics in the saturated regime at a drain-to-source voltage (V_{DS}) of 40 V. The SnGaO films were patterned to be narrower than the source-drain electrodes to avoid current spreading [Fig. 2(c)] and to ensure a reliable estimation of the field-effect mobility. As the Ga ratio increased, the on current (I_{on}) decreased, and the subthreshold region drifted in the positive direction. Devices with a Ga ratio of 50.0% fabricated on the same wafer with different channel lengths (100, 150, 200, 250, 300, and 350 μm) and a fixed channel width (1000 μm) were randomly selected and measured [Fig. 2(e)], showing generally good uniformity. A dual scan of the transfer curves and the output characteristics for TFTs with various compositional ratios are shown in Fig. 3. In the output curves, I_D exhibits a good linear relation at small values of V_{DS} (from 0 to 5 V), confirming good ohmic contact.

The electrical parameters including saturation mobility (μ_{sat}), threshold voltage (V_{th}), subthreshold slope (SS), and on-off current ratio (I_{on}/I_{off}) were extracted [Fig. 4(a)]. The values of saturated mobility μ_{sat} in the saturation region (V_{DS} = 40 V) are extracted from Ref. 27 as follows: $I_{DS} = \left(\frac{\mu_{sat} W C_i}{2L}\right)(V_{GS} - V_{th})^2$, where C_i, W, and L are the capacitance of the gate dielectric per unit area, channel width, and channel length, respectively. The values of V_{th} were extrapolated as the intercept by the linear fitting between a function H and V_{GS} according to the equation $H(V_{GS}) = \frac{(V_{GS} - V_{th})}{m+1}$, where $H(V_{GS}) = \frac{\int_0^{V_{GS}} I_{DS}(V_{GS}) dV_{GS}}{I_{DS}}$ and $I_{DS} = K(V_{GS} - V_{th})^m$ (K is a conductance parameter with units of AV^{-m} and m is an empirical parameter which can be different from 2).[28,29] Here, some of the devices turn on at negative V_{GS} values and thus we integrate from V_{GS0}, where the devices start to turn on, instead of zero. With the increasing Ga ratio, μ_{sat} decreased from 9.82 to 0.66 cm^2/V s (where

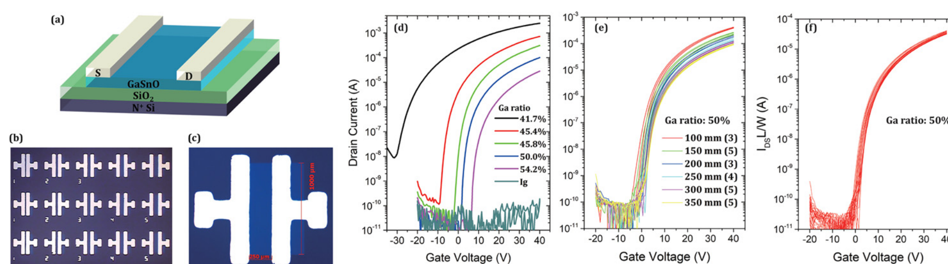

FIG. 2. (a) A schematic representation of the cross-sectional view of SnGaO TFTs. (b) Optical micrograph of the fabricated TFTs. (c) A zoomed-in image of a device. (d) Transfer characteristics in the saturated regime (V_{DS} = 40 V) for SnGaO TFTs with different compositional ratios. (e) The transfer characteristics of 25 randomly selected devices with different channel lengths (100, 150, 200, 250, 300, or 350 μm) and the same channel width (1000 μm) on a sample with the Ga ratio of 50.0% in the film. (f) The drain current in (e) was normalized by multiplying W/L.

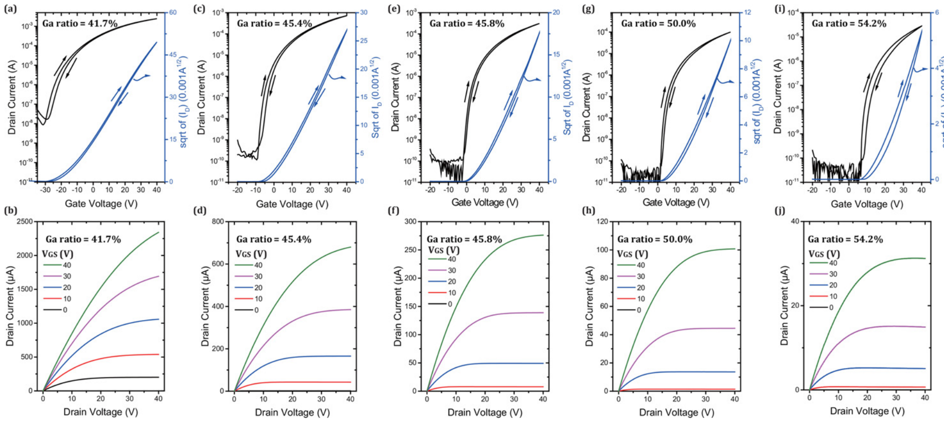

FIG. 3. The measured transfer and output characteristics in the saturation region (V_{DS} = 40 V) of SnGaO TFTs with different Ga ratios: (a) and (b) 41.7%, (c) and (d) 45.4%, (e) and (f) 45.8%, (g) and (h) 50.0%, and (i) and (j) 54.2%.

μ_{sat} is the average mobility in the range of $V_{GS} - V_{th} = 33$–35 V), V_{th} positively shifted from −28.25 to 4.93 V, the on current decreased from 2.5×10^{-3} to 2.8×10^{-5} A, I_{off} decreased from 1.7×10^{-8} to 5.3×10^{-11} A, and the *SS* decreased from 2.52 to 0.65 V/dec. These evolutions are similar to those obtained for Ga-doped indium oxide TFTs[30] and IGZO TFTs,[31] which is attributed to the fact that Ga suppresses oxygen vacancies and reduces the carrier concentration.

The transfer curves in the linear region (V_{DS} = 0.1 V) can be used to reveal the electron transport properties by plotting the differential field-effect mobility as a function of ($V_{GS} - V_{th}$)[32] [Fig. 4(b)]. Generally, the curves almost follow the power law $\mu \sim (V_{GS} - V_{th})^{\gamma}$, and it indicates the existence of localized states below the conduction band edge, following the typical trap-limited and percolation transport observed in InGaZnO TFTs.[33] Considering that the vacuum-processed SnGaO TFTs exhibited a high mobility of 25.6 cm^2/V s (Ref. 21), such an observation may imply that the device performance can be further enhanced by optimizing the processing, such as using high-*k* dielectrics composed of oxide materials,[34] doping carrier suppressors like Hf, Y, Zr, and Al with a lower standard electrode potential (SEP),[35] fabrication via combustion processing,[36] and UV irradiation assisted annealing.[37]

Moreover, the *SS* values are related to the total trap density (N_t), which includes the bulk trap density in the active layer and the interface trap density at the semiconductor-dielectric interface during scanning.[38] That is:[12] $N_t = \left[\frac{q \cdot SS \cdot \log(e)}{kT} - 1\right]\frac{C_i}{q}$. Here, *k*, *T*, and *q* are the Boltzmann constant, absolute temperature, and electron charge, respectively. The SnGaO TFT with 50.0% Ga exhibits the smallest *SS* of 0.60 V/decade and a low trap density (1.95×10^{12} cm^{-2}), whereas the device with the smallest Ga ratio (41.7%) exhibits the largest *SS* (2.52 V/dec) corresponding to a high trap density (8.91×10^{12} cm^{-2}), probably related to the presence of more oxygen vacancies with a lower Ga content.

The evolution of the oxygen vacancies was further investigated by XPS analysis (Fig. 5), and the asymmetric peak of the O1s spectrum can be deconvoluted into three peaks:[39] (1) The low binding energy (O_I) side at 530.6 eV is attributed to O^{2-} ions combined with Ga or Sn ions; (2) The peak at the medium binding energy O_{II} is assigned to O^{2-} ions in the oxygen-deficient regions; (3) The high binding energy component O_{III} is related to loosely bound oxygen, such as chemisorbed surface hydroxyl, -CO_3, absorbed H_2O, or absorbed O_2.[40,41] In particular, the area under the O_{II} peak is proportional to the concentration of oxygen vacancies (V_O), which act as carrier sources.[42] As the Ga content increases, the ratio of the O_{II} peak area to that of the total oxygen region decreases from 30.46% to 17.52%, manifesting that Ga suppresses oxygen vacancies and reduces the

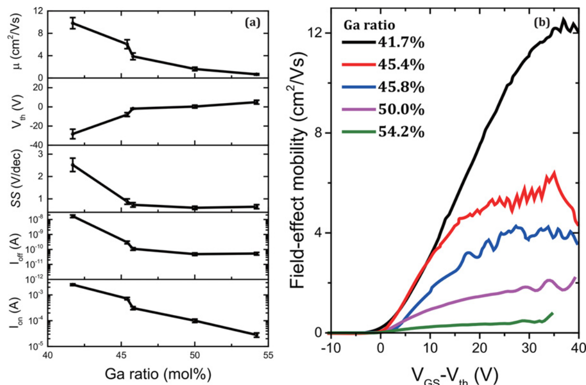

FIG. 4. (a) The effect of the Ga ratios on the electrical properties in the saturation region (V_{DS} = 40 V) of SnGaO TFTs. (b) Mobility as a function of ($V_{GS} - V_{th}$) in the linear region (V_{DS} = 0.1 V) for the devices made from the films with the Ga ratio of 41.7%, 45.4%, 45.8%, 50.0%, and 54.2%.

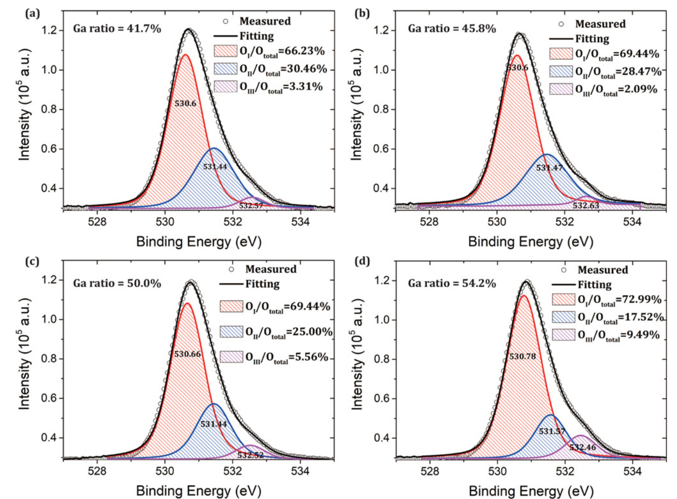

FIG. 5. The XPS spectrum for the O1s peaks and their deconvolution results for SnGaO films with different Ga ratios: (a) 41.7% and O_{II}/O_{total} = 30.46%, (b) 45.8% and O_{II}/O_{total} = 28.47%, (c) 50.0% and O_{II}/O_{total} = 25.00%, and (d) 54.2% and O_{II}/O_{total} = 17.52%.

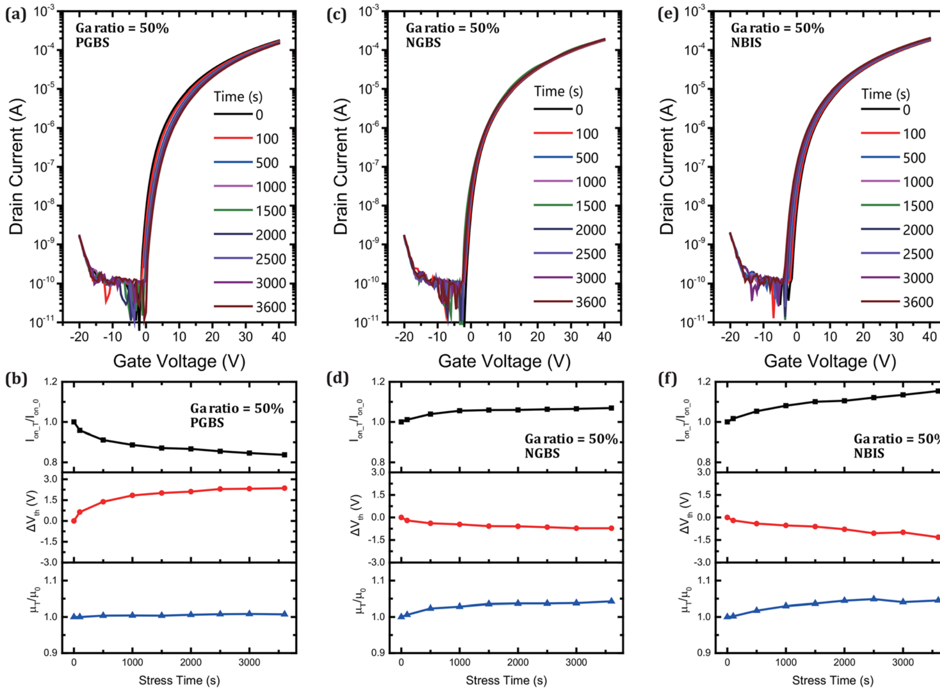

FIG. 6. The transfer characteristics and the evolution of the characteristic parameters as a function of stressing time in the saturation region ($V_{DS} = 40\,V$) for SnGaO TFTs with a Ga ratio of 50.0%: (a) and (b) under PGBS, (c) and (d) under NGBS, and (e) and (f) under NBIS. The parameters include I_{on_T}/I_{on_0}, ΔV_{th}, and μ_T/μ_0, where subscripts T and 0 denote the final and initial states, respectively.

carrier concentration. The smaller ratio for the O_{II} peak area to the total oxygen region is usually attributed to fewer donor-like states that release free carriers to the conduction levels.[43] According to the typical models for trap-limited and percolation transport, more free carriers result in a higher ratio of mobile carriers to total carriers (including mobile states above the conduction level and immobile states below it) and thus a higher field-effect mobility under gate tuning.

For gate bias stress stability testing, we focused on SnGaO TFT devices showing an on-voltage close to zero, i.e., the device with a Ga ratio of 50.0% (Fig. 6). The device stability was tested under stress in air after coating a layer of polymer CYTOP for simple encapsulation. The evolution of parameters including the shift in V_{th} (ΔV_{th}), I_{on}, and μ_{sat} in the saturation region ($V_{DS} = 40\,V$) is shown under positive gate bias stress (PGBS), negative gate bias stress (NGBS), and negative gate bias stress with illumination (NBIS), where the on current and saturated mobility were normalized to the original peak values ($t = 0$ s) for comparison. The values of V_{th} were also extracted as stated above and the gate bias is 20 V and −20 V for PGBS and NGBS, respectively. The NBIS is measured by applying a negative bias (−20 V) under white light. I_{on} drops slightly from 1.76×10^{-4} A to 1.47×10^{-4} A under PGBS, rises negligibly under NGBS, and rises from 1.76×10^{-4} A to 2.03×10^{-4} A under NBIS. The shift in V_{th} is 2.36 V, −0.72 V, and −1.32 V for PGBS, NGBS, and NBIS, respectively, with no obvious change in the mobility. Also, we measured the gate bias stress stability of the SnGaO TFTs without CYTOP encapsulation, which shows a shift of 3.94 V, −1.03 V, and −5.24 V in V_{th} for PGBS, NGBS, and NBIS, respectively. The encapsulation layers improve the long-term stability in stressing due to preventing water or oxygen adsorption, but they did not reduce the hysteresis in dual scanning, which is probably related to electron trapping at the semiconductor-insulator interface.[44,45] For comparison, the stability test results obtained for the sol-gel-based InGaZnO TFTs fabricated at the same conditions exhibit a ΔV_{th} of 6.36 V and −6.67 V under PGBS and NGBS, respectively. The SnGaO TFT shows a smaller change in the trend for I_{on} and μ_{sat} under gate bias stress, exhibiting a better stability that is most likely due to the elimination of the weaker Zn-O bonds. For a reference, solution-processed ZnSnO TFT showed a ΔV_{th} of 5.82 V under PGBS.[11] The NBIS results show little change compared to the NGBS results, suggesting that the SnGaO has low response to white light, probably owing to the large bandgap. The V_{th} shifts under the gate bias stress can be attributed to the formation of deep defect traps that capture charges at the interface between the channel and the dielectric and the absorption of O_2 from the ambient atmosphere onto the back-channel surface.[46] Apparently, Ga ion is an efficient oxygen binder for the SnGaO system, which may prevent the creation of oxygen vacancy defects that are active toward the gate bias stress.

Compared with other Sn-based oxide semiconductor TFTs,[14,15,19–21] which are mostly quaternary compounds including element Zn or fabricated by the high-cost vacuum process, the demonstrated SnGaO is a Zn-free ternary compound and fabricated by the solution process and also shows a good stability, which may merit considerations for simple fabrication of oxide transistors.

In summary, we investigated the dependence of the SnGaO TFT characteristics on the compositional ratio along with the information of oxygen vacancies. As the Ga ratio increased, the on current for the SnGaO TFTs decreased, which was mainly related to the drop in the carrier concentration. The average field-effect mobility of the SnGaO TFTs could be tuned from 0.67 to 9.82 $cm^2/V\,s$ and the on-off ratio is more than 10^6 with good stability in different bias-stressing conditions, probably due to the strong Ga-O bonds. The introduction of Ga allows fine tuning of electrical performance and the capability of solution-processed patterning by selective etching, which may provide new opportunities

and understandings for solution-based and transparent tin-oxide and gallium-oxide electronics.

The authors gratefully acknowledge the financial support of the project from the National Natural Science Foundation of China (61774174) and Guangdong Provincial Department of Science and Technology (2015B090924001). B.L. acknowledges the support of the Natural Science Foundation of China (NSFC) for the Youth Scientist grant (Grant No. NSFC 11504309) and the Early Career Scheme (ECS) Fund (Grant No. PolyU 253026/16P) from the Research Grant Council (RGC) in Hong Kong.

[1]E. Fortunato, P. Barquinha, and R. Martins, Adv. Mater. **24**(22), 2945–2986 (2012).
[2]H. Pu, Q. Zhou, L. Yue, and Q. Zhang, Semicond. Sci. Tech. **28**(10), 105002 (2013).
[3]K. Nomura, H. Ohta, A. Takagi, T. Kamiya, M. Hirano, and H. Hosono, Nature **432**(7016), 488 (2004).
[4]M. Li, J. Zheng, H. Xu, Z. Wang, Q. Wu, B. Huang, H. Zhou, and C. Liu, Adv. Mater. Interfaces **5**(1), 1700981 (2018).
[5]H.-C. Cheng and C.-Y. Tsay, J. Alloys Compd. **507**(1), L1–L3 (2010).
[6]K. B. Park, J. B. Seon, G. H. Kim, M. Yang, B. Koo, H. J. Kim, M. K. Ryu, and S. Y. Lee, IEEE Electron Device Lett. **31**(4), 311–313 (2010).
[7]A. Liu, G. X. Liu, H. H. Zhu, F. Xu, E. Fortunato, R. Martins, and F. K. Shan, ACS Appl. Mater. Interfaces **6**(20), 17364–17369 (2014).
[8]H. Li, M. Qu, and Q. Zhang, IEEE Electron Device Lett. **34**(10), 1268–1270 (2013).
[9]B. D. Ahn, H. J. Jeon, J. Sheng, J. Park, and J. S. Park, Semicond. Sci. Tech. **30**(6), 064001 (2015).
[10]Y. J. Chang, D. H. Lee, G. S. Herman, and C. H. Chang, Electrochem. Solid-State Lett. **10**(5), H135–H138 (2007).
[11]S. J. Seo, C. G. Choi, Y. H. Hwang, and B. S. Bae, J. Phys. D: Appl. Phys. **42**(3), 35106–35105 (2009).
[12]Y. S. Rim, D. L. Kim, W. H. Jeong, and H. J. Kim, Electrochem. Solid-State Lett. **15**(2), H37–H40 (2012).
[13]H. Kim and W. S. Choi, Ceram. Int. **43**(6), 4775–4779 (2017).
[14]J. Li, C. X. Huang, J. H. Zhang, W. Q. Zhu, X. Y. Jiang, and Z. L. Zhang, Mater. Res. Bull. **68**, 22–26 (2015).
[15]H. B. Kim and H. S. Lee, Thin Solid Films **550**, 504–508 (2014).
[16]T. Kamiya, K. Nomura, and H. Hosono, Phys. Status Solidi A **207**(7), 1698–1703 (2010).
[17]I. Tanaka, F. Oba, K. Tatsumi, M. Kunisu, M. Nakano, and H. Adachi, Mater. Trans. **43**(7), 1426–1429 (2002).
[18]Z. Hajnal, J. Miró, G. Kiss, F. Réti, P. Deák, R. C. Herndon, and J. M. Kuperberg, J. Appl. Phys. **86**(7), 3792–3796 (1999).
[19]D.-S. Han, J.-H. Park, Y.-J. Kang, and J.-W. Park, Microelectron. Reliab. **53**(12), 1875–1878 (2013).
[20]J. Yang, T. Meng, Z. Yang, C. Cui, and Q. Zhang, J. Phys. D: Appl. Phys. **48**(43), 435108 (2015).
[21]T. Matsuda, K. Umeda, Y. Kato, D. Nishimoto, M. Furuta, and M. Kimura, Sci. Rep. **7**, 44326 (2017).
[22]M. Takahashi, H. Kishida, A. Miyanaga, and S. Yamazaki, "Theoretical analysis of IGZO transparent amorphous oxide semiconductor," paper presented at the IDW '08 - Proceedings of the 15th International Display Workshops, 2008.
[23]N. Serpone, D. Lawless, and R. Khairutdinov, J. Phys. Chem. **99**(45), 16646–16654 (1995).
[24]M. Batzill and U. Diebold, Prog. Surf. Sci. **79**(2–4), 47–154 (2005).
[25]M. Higashiwaki, K. Sasaki, A. Kuramata, T. Masui, and S. Yamakoshi, Appl. Phys. Lett. **100**(1), 013504 (2012).
[26]S. Hwang, J. H. Lee, C. H. Woo, J. Y. Lee, and H. K. Cho, Thin Solid Films **519**(15), 5146–5149 (2011).
[27]D. K. Schroder, *Semiconductor Material and Device Characterization* (John Wiley & Sons, 2006).
[28]A. Ortiz-Conde, F. G. Sánchez, J. J. Liou, A. Cerdeira, M. Estrada, and Y. Yue, Microelectron. Reliab. **42**(4–5), 583–596 (2002).
[29]A. Ortiz-Conde, F. J. García-Sánchez, J. Muci, A. T. Barrios, J. J. Liou, and C.-S. Ho, Microelectron. Reliab. **53**(1), 90–104 (2013).
[30]J. H. Park, W. J. Choi, S. S. Chae, J. Y. Oh, S. J. Lee, K. M. Song, and H. K. Baik, Jpn. J. Appl. Phys., Part 1 **50**(8), 080202 (2011).
[31]D. H. Lee, S. M. Park, D. K. Kim, Y. S. Lim, and M. Yi, J. Semicond. Tech. Sci. **14**(2), 163–168 (2014).
[32]Y. Kang, B. D. Ahn, J. H. Song, Y. G. Mo, H. H. Nahm, S. Han, and J. K. Jeong, Adv. Electron. Mater. **1**(7), 1400006 (2015).
[33]S. Lee, K. Ghaffarzadeh, A. Nathan, J. Robertson, S. Jeon, C. Kim, I. H. Song, and U. I. Chung, Appl. Phys. Lett. **98**(20), 203508 (2011).
[34]A. Zeumault and V. Subramanian, Adv. Funct. Mater. **26**(6), 955–963 (2016).
[35]S. J. Kim, S. Yoon, and H. J. Kim, Jpn. J. Appl. Phys., Part 1 **53**(2S), 02BA02 (2014).
[36]M.-G. Kim, M. G. Kanatzidis, A. Facchetti, and T. J. Marks, Nat. Mater. **10**(5), 382 (2011).
[37]Y.-H. Kim, J.-S. Heo, T.-H. Kim, S. Park, M.-H. Yoon, J. Kim, M. S. Oh, G.-R. Yi, Y.-Y. Noh, and S. K. Park, Nature **489**(7414), 128 (2012).
[38]E. N. Cho, J. H. Kang, and I. Yun, Microelectron. Reliab. **51**(9–11), 1792–1795 (2011).
[39]S. Ullah Awan, S. Hasanain, M. F. Bertino, and G. Hassnain Jaffari, J. Appl. Phys. **112**(10), 103924 (2012).
[40]M. Chen, X. Wang, Y. Yu, Z. Pei, X. Bai, C. Sun, R. Huang, and L. Wen, Appl. Surf. Sci. **158**(1–2), 134–140 (2000).
[41]J. W. Hennek, J. Smith, A. Yan, M.-G. Kim, W. Zhao, V. P. Dravid, A. Facchetti, and T. J. Marks, J. Am. Chem. Soc. **135**(29), 10729–10741 (2013).
[42]Q. Jiang, L. Feng, C. Wu, R. Sun, X. Li, B. Lu, Z. Ye, and J. Lu, Appl. Phys. Lett. **106**(5), 053503 (2015).
[43]G. Li, B.-R. Yang, C. Liu, C.-Y. Lee, Y.-C. Wu, P.-Y. Lu, S. Deng, H.-P. D. Shieh, and N. Xu, IEEE Electron Device Lett. **37**(5), 607–610 (2016).
[44]J. Raja, K. Jang, H. H. Nguyen, T. T. Trinh, W. Choi, and J. Yi, Curr. Appl. Phys. **13**(1), 246–251 (2013).
[45]C. H. Ahn, B. H. Kong, H. Kim, and H. K. Cho, J. Electrochem. Soc. **158**(2), H170–H173 (2011).
[46]M. Matters, D. M. D. Leeuw, P. T. Herwig, and A. R. Brown, Synth. Met. **102**(1), 998–999 (1999).